Metals and Materials International (2020) 26:1036–1044
https://doi.org/10.1007/s12540-019-00539-1

# Metallurgical Assessment of Novel Mg–Sn–La Alloys Produced by High-Pressure Die Casting

**Azim Gökçe**[1,2]

Received: 1 October 2019 / Accepted: 7 November 2019 / Published online: 12 November 2019


**Abstract**
Mg alloys containing Al are widely used for industrial applications, but the use of these alloys as an automotive part is limited due to the low melting temperature of the $Mg_{17}Al_{12}$ intermetallic phase. Therefore, magnesium alloys without aluminum that can withstand higher operating temperatures are of interest to the automotive industry. The objective of this work is to develop Al-free Mg alloys for industrial applications. In the current work, four types of alloys were produced with varying La contents. The high-pressure die casting method was selected to overcome the problems inherent in the gravity casting method with respect to the production of parts with complex shapes and thin walls. X-ray diffraction analysis revealed that the base alloy (Mg–5Sn wt%) comprises of α-Mg and $Mg_2Sn$ phases whereas La containing alloys included intermetallic phases such as $LaMg_3$, $Mg_{17}La_2$, and $La_5Sn_3$. Corresponding grain sizes of the alloys with La are lower than those of the Mg5Sn alloy. Due to this lower grain size and emerging dispersoids, the tensile strength of the Mg5Sn4La alloy (205 MPa) is roughly double that of Mg5Sn. Moreover, the addition of the 4% wt. La to the Mg5Sn alloys led to an increase in yield strength and ductility by 25% and 50%, respectively.

**Keywords** Magnesium · Microscopy · High-pressure die casting · Light alloys · Mechanical properties

## 1 Introduction

The increase in demand for thin wall structures and complex shapes has led the automotive industry to use alternative manufacturing techniques instead of sand casting [1]. High-pressure die casting (HPDC) is one of the methods used to overcome the aforementioned limitations of sand casting. This method also offers higher production speed and lower cost compared to other processes [2]. Using HPDC, parts weighing from a few grams to over 15 kg can be produced; in addition, the method is highly adaptable to automation and mass production [3].

Aluminum, magnesium, and titanium are the most common industrial alloys termed as "light-alloys" [4]. It is stated that roughly half of the light metal cast parts produced in the world are produced by HPDC [2]. Magnesium stands out from other light alloys due to its low density, high specific strength, good castability and weldability [5, 6]. Also, it is reported that Mg can be used to improve the energy efficiency and system performance in aerospace, transportation, defense, electronics and biomedical applications [7]. Recent regulations from the EU commission with respect to greenhouse gas emissions have forced vehicle manufacturers to produce lighter vehicles [8–10]. Magnesium is 75% lighter than steel and 35% lighter than aluminum; therefore, a significant reduction in vehicle weight can be achieved through the use of magnesium in the framework and panel production [11]. However, the tensile strength (as cast: ~ 85 MPa [12]) and elongation (2%–8% [13]) of pure magnesium are considerably lower than that required for use in automotive manufacturing. Aluminum and zinc are the most commonly used alloying elements to increase the strength of magnesium [14]. AZ91 (9 wt% Al, 1 wt% Zn) and AM60 (6 wt% Al, 0.2 wt% Mn) are the most preferred Mg alloys, constituting 90% of the magnesium alloys used in structural applications [15]. However, the biggest handicap of Mg–Al alloys is the low melting temperature (427 °C) of the $Mg_{17}Al_{12}$

✉ Azim Gökçe
azimg@sakarya.edu.tr

[1] Materials Innovation Guild, Mechanical Engineering Department, Speed School of Engineering, University of Louisville, Louisville, KY 40217, USA

[2] Metallurgy and Materials Engineering Department, Technology Faculty, Sakarya University of Applied Sciences, 54187 Sakarya, Turkey

intermetallic phase which forms during solidification [16]. Moreover, Polmear [17] revealed that the incompatibility of the lattice systems of Mg (HCP) and $Mg_{17}Al_{12}$ (BCC) causes the fragility of the interfaces of these constituents and detrimentally affects the ductility property of Mg alloys containing Al. Lü et al. [18] stated that microcracks tend to form in the $Mg/Mg_{17}Al_{12}$ interface and that the volume and morphology of $Mg_{17}Al_{12}$ have significant effects on the mechanical properties of Mg–Al alloys. However, as the composition of the Mg–Al alloys approaches the eutectic composition, the strength, and castability of the Mg–Al alloys increases, although the increasing Al amount causes a reduction in ductility [19]. So, it is expected that alloys which have less Al content will have higher ductility values resulting in a demand for new alloys without Al. Sn is one of the elements considered to be a substitute for Al in Mg alloys. Intermetallic-phase $Mg_2Sn$ forms when Mg is alloyed with Sn instead of Al; the melting point of this phase is about 770 °C. This situation ensures that the high-temperature properties of Mg-Sn alloys are superior to those of Mg–Al alloys [20]. Furthermore, Liu et al. [12] stated that the maximum solidification range of Mg–Sn alloys is narrower than that of Mg–Al alloys, so their tendency to form casting defects, such as hot tear and dispersed shrinkage, is lower than that of Mg–Al alloys. Moreover, the solid solubility of the Sn in the Mg at 561 °C is 85 times higher than its solubility at room temperature. Therefore Mg–Sn alloys could be strengthened via precipitation hardening.

Gupta et al. [21] reported that Rare Earth (RE) elements have positive effects on the properties of Mg alloys. Feyerabend et al. [22] observed that it is possible to achieve a 50% increase in tensile strength of the gravity-casted Mg alloy with the addition of 15% wt Gd. Another study [23] showed that the addition of La or Nd to the HPDC Mg causes a notable increase in the creep performance of the Mg alloy. Multiple studies on the combined effects of La, Nd, Ce [24–26] and La, Nd, Ce, Pr [27–29] on the performance of the HPDC processed Mg alloys, reported that a certain amount of the RE addition enhances the mechanical properties of the HPDC Mg alloys.

Another alloy system that attracts the researchers' attention is the Mg–Sn–RE ternary alloys. Zhao et al. [30] investigated the effects of Y addition on the properties of the Mg–Sn alloy and stated that MgSnY and $Sn_3Y_5$ type dispersoids enhance mechanical properties. Additionally, Wang et al. [31] reported that the addition of more than 2% wt Y has a detrimental effect on the ductility of the Mg–Sn alloys due to coarsening of the dispersoids. Similarly, MgSnCe type intermetallics with a rod-like shape are considered as the main strengthening constituents of as-cast Mg–Sn–Ce alloys [32]. Sevik et al. [33] investigated the effects of Ce addition on the properties of HPDC processed Mg5Sn alloy and observed that Ce addition decreases grain size and increases tensile strength. Huang et al. [34] reported that the addition of Nd into an Mg–Sn alloy weakens the dendrites. It is reported that the addition of Gd to the Mg–3Sn alloy leads to higher mechanical properties when the amount of Gd is lower than 1.34 wt% [35]. The alloy's mechanical properties weaken due to the formation of feather-like brittle MgSnGd intermetallic constituents when the amount of the Gd is over the mentioned amount. Jiang et al. [36] investigated the effect of Yb addition on $Mg_2Sn$ alloy and reported the formation of $Mg_2$(Sn,Yb) type phases and the precipitation of them along grain boundaries. In brief, all the studies based on Mg-Sn-RE systems reported the enhancement of the properties through the mechanisms of grain refinement, solid solution strengthening or precipitation strengthening. However, there exists a lack of literature on HPDC processed Mg-Sn-La ternary alloys. As such, the objective of this study is to produce novel HPDC Mg-Sn alloys without Al and to perform a metallurgical assessment of the effects of La content on the properties of the emerging alloys.

## 2 Experimental details

An induction furnace was used to prepare the alloys with the chemical composition given in Table 1. Pure Mg, pure Sn, and Mg–30La master alloy ingots were smelted in a SiC crucible under a protective atmosphere (2% $SF_6$ + 98% $CO_2$) to prevent oxidation during the smelting process. Once the pure Mg metal was heated to a temperature of 730 °C, Mg-La master alloy was added to the crucible. Sn was added to the smelted Mg–La mixture just before the casting to prevent its evaporation due to its low melting temperature. The HPDC mold was heated to a temperature of 200 °C prior to the casting process. The melted alloy was poured into the mold with a clamping force of 76 kN. Using the available mold geometry, 4 tensile specimens (Fig. 1-T) and microstructure samples (Fig. 1-M) were produced in each casting process.

Tensile tests were carried out in accordance with the ASTM E8 M standard. An axial clip-on extensometer (Epsilon 3542) was used to measure the elongation. Four tests were conducted and the average value recognized as the tensile strength of the investigated alloy. The apparent hardness of the alloys was determined using the Brinell scale with

**Table 1** Chemical compositions of the investigated alloys

| Alloy code | Composition (wt%) | | |
|---|---|---|---|
| | Mg | Sn | La |
| Mg5Sn | 95 | 5 | 0 |
| Mg5Sn1La | 94 | 5 | 1 |
| Mg5Sn2La | 93 | 5 | 2 |
| Mg5Sn4La | 91 | 5 | 4 |


**Fig. 1** High-pressure die-cast specimens

an applied force of 31.25 kg. A minimum of 10 readings was recorded to assess the hardness of each alloy. Microstructural analysis was conducted using a combination of Optical Microscopy (Nikon Eclipse L50), Scanning Electron Microscopy (JEOL-JSM 6060LV), and X-ray Diffraction (Rigaku-D/Max 2200). Standard metallographic techniques were used to prepare the specimens for the microstructural analyses. However, final polishing was carried out using 0.05 µm Colloidal silica. An IXRF 500 Energy Dispersive Spectroscopy (EDS) analysis device was used to analyze the elemental composition of the constituents detected by SEM. It should be noted that oxygen content was excluded from the EDS analyses. The alloys' grain sizes were measured under polarized light using Clemex Image Analyzing software coupled with the optical microscope.

## 3 Results and discussion

The alloys grain size as a function of La content is provided in Fig. 2. It is clearly seen from Fig. 2 that La acts as a grain refiner due to the higher melting temperature of La containing intermetallic phases. It is assumed that the addition of La caused the formation of nucleation sites at higher temperatures during solidification. According to the La-Sn phase diagram [37], the melting temperature of the $La_5Sn_3$ phase is ~ 1500 °C, highlighting the formation of $La_5Sn_3$ nucleates. Thus, it is expected that higher La content leads to smaller grain sizes. However, error bars of the grain size measurements (Fig. 2) reveal the presence of an excessive difference between the minimum and maximum grain size values. Bowles et al. [38] stated that such a situation is very common in the HPDC process due to different cross-sections of the casted part and high plastic deformation rates. The shortest error bar is reached in the alloy with 4% wt. La addition; this is considered to be proof of the inoculation effect of La.

A decrease in the grain sizes as La content increases is clearly visible on the SEM images of the investigated alloys (Fig. 3). It is worth noting that fine equiaxed grains of α-Mg are readily seen in all circumstances. As mentioned previously, some of the grains which are bigger than average ones, are also noteworthy. It should be noted that submicron grains are observed on the white-colored areas of the Mg5Sn4La alloy; however, it is not possible to reveal these grains at this level of magnification. However, these constituents will be studied in the later part of the paper.

The SEM image of the Mg5Sn alloy (Fig. 4) revealed the presence of the intergranular network of the eutectic

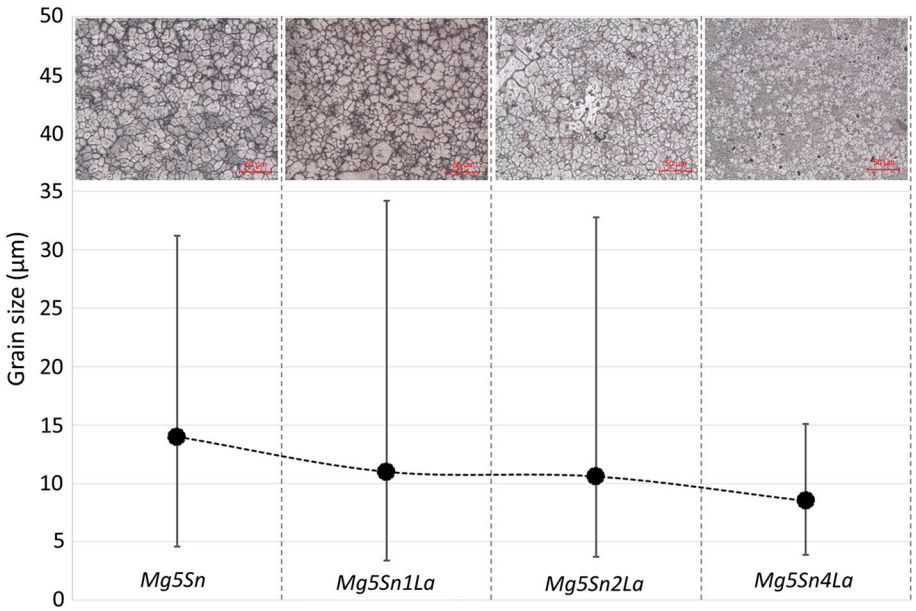


**Fig. 2** Optical micrographs and grain size values of the alloys as a function of La content. Error bars show the minimum and maximum grain sizes measured

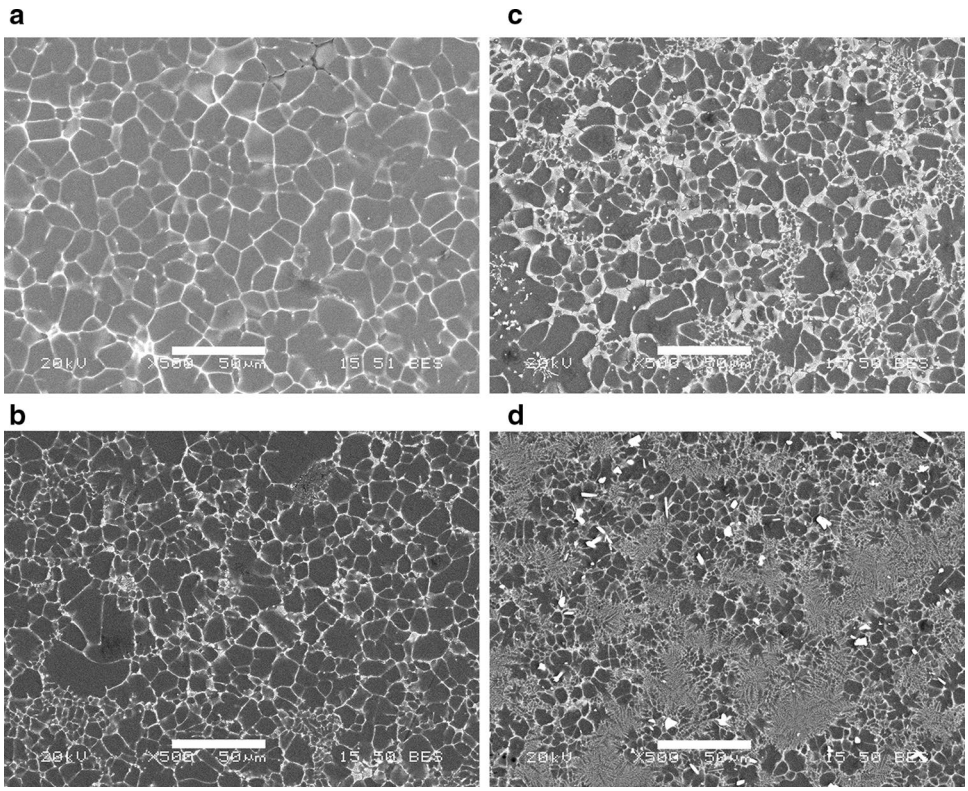


**Fig. 3** SEM images of the investigated alloys. **a** Mg5Sn, **b** Mg5Sn1La, **c** Mg5Sn2La, **d** Mg5Sn4La

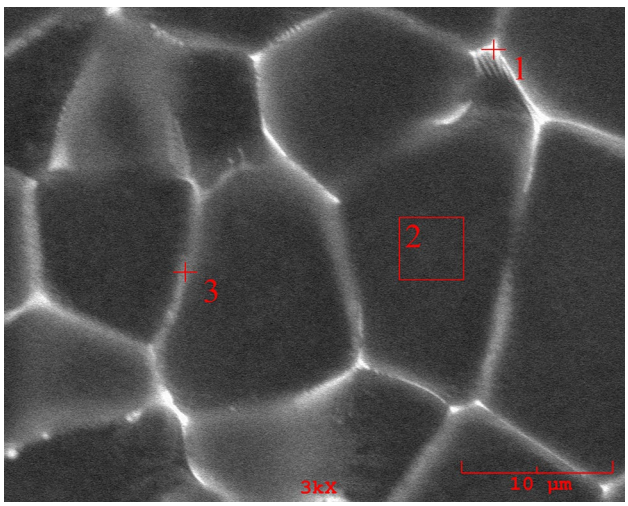


**Fig. 4** SEM image of the Mg5Sn alloy

**Table 2** EDX analyses recorded at the point locations shown in Fig. 4

| Point | Element (wt%) | | |
|---|---|---|---|
| | Mg | Sn | O |
| 1 | 81.313 | 12.705 | 5.982 |
| 2 | 93.811 | 1.969 | 4.220 |
| 3 | 90.731 | 6.250 | 3.019 |

phase. It is well known that elements with higher atomic mass have a brighter appearance on SEM images taken in backscattered electron mode [39]. Thus, it is thought that the intergranular phase in Fig. 4 contains a higher Sn content than that of the matrix phase. EDX analysis was conducted to identify the exact chemical composition of the Mg5Sn alloy, and the results of the analysis are reported in Table 2. Figure 4, Point 1 and Point 3 represent the intergranular zones; it is clearly seen that these points are enriched with Sn. Since Point 1 contains a higher amount of Sn (Table 2) than the other two points, it has a brighter color. The binary phase diagram for Mg-Sn indicates that the $Mg_2Sn$ phase forms when Mg is alloyed with Sn [40]. The eutectic melting temperature for Mg-rich Mg–Sn binary alloys is 570 °C, so this phase is the last solidified constituent during solidification of the mentioned alloys. It was therefore concluded that the intermetallic phase of the $Mg_2Sn$ alloy is formed in the intergranular zones of the Mg5Sn alloy [33, 41]. The matrix of the alloy consists of Mg and Sn; however, the amount of the Mg is lower than that of the intergranular phases. O was detected on all the analyzed points and is attributed to the surface oxide formed due to magnesium's high affinity towards oxygen.

It was observed that some laminated structures were formed with the addition of La to the Mg5Sn alloy (Fig. 5). The amount of the laminates increases with an increase in La content, so it is thought that these laminates contain La. Hence, EDS analysis (Table 3) indicated that these laminates (Fig. 5a, Points 1 and 4, Fig. 5b, Points 2 and 3) contain a

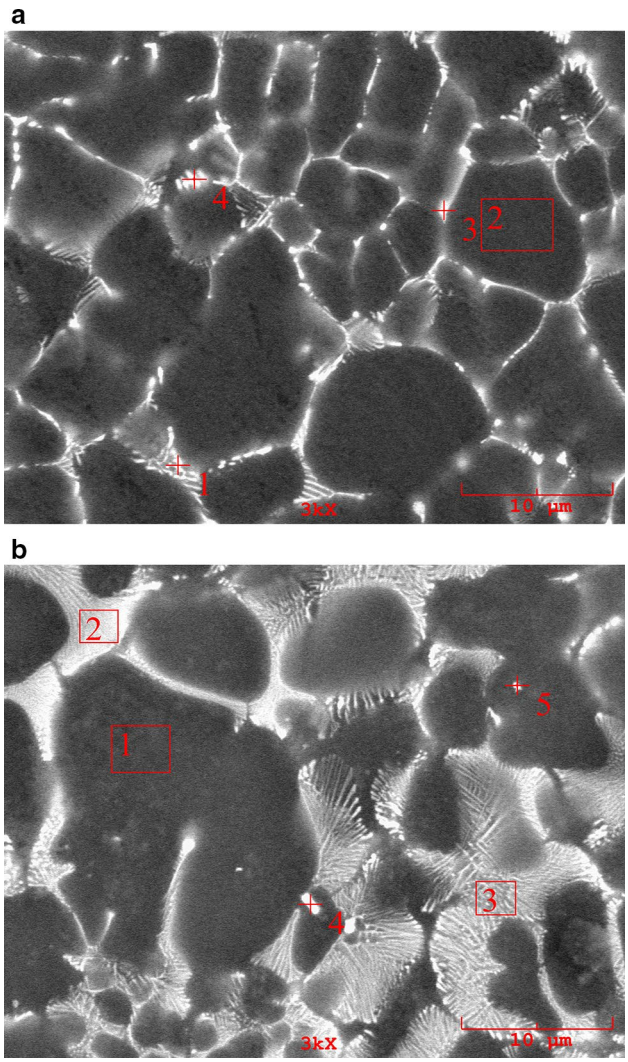


**Fig. 5** SEM image of **a** Mg5Sn1La, **b** Mg5Sn2La alloys

**Table 3** EDX analysis results corresponding to the point locations shown in Fig. 5

| Alloy | Point | Element (wt%) | | | |
|---|---|---|---|---|---|
| | | Mg | Sn | La | O |
| Mg5Sn1La | 1 | 90.150 | 7.263 | 2.587 | – |
| | 2 | 94.154 | 1.1412 | 0.627 | 3.806 |
| | 3 | 86.285 | 11.899 | 1.816 | – |
| | 4 | 83.527 | 9.240 | 4.003 | 3.230 |
| Mg5Sn2La | 1 | 92.236 | 0.975 | 0.851 | 5.939 |
| | 2 | 80.994 | 7.759 | 5.168 | 6.079 |
| | 3 | 83.438 | 6.977 | 4.345 | 5.240 |
| | 4 | 78.456 | 9.478 | 8.358 | 3.707 |
| | 5 | 89.542 | 2.752 | 3.889 | 3.817 |

higher amount of La compared to the matrix. Furthermore, since La was detected in the matrix of Mg5Sn1La (Fig. 5a, Point 2) and Mg5Sn2La (Fig. 5b-Point 1) alloys, it is thought that the matrix consists of a solid solution of binary Mg-Sn and Mg-La based intermetallic phases. The binary Mg-La phase diagram [42] indicates that the solubility of La in α-Mg is very low at room temperature.

XRD analysis was used to identify the phases formed during solidification of the alloys. As previously stated, in the Mg5Sn alloy the only phases detected were α-Mg (International Center for Diffraction Data-ICDD No: 01-089-4894) and $Mg_2Sn$ (ICDD No: 03-065-2997) (Fig. 6). The absence of the elemental Sn proves that Sn is fully diffused through the Mg matrix. Wei et al. reported the presence of these mentioned phases in their study on the gravity cast Mg–5Sn alloy [43]. It is apparent that the 1% La addition caused the formation of a new type of phase, $Mg_{17}La_2$ (ICDD No: 00-017-0399). According to the Mg–Al phase diagram, when Mg is alloyed with La the microstructure of the alloy consisted of an α-Mg + $Mg_{17}La_2$ solid solution. However, when La content was increased to 2% wt, a small portion of the $La_5Sn_3$ (ICDD No: 00-033-0725) phase was detected and the peak height of this phase increased when the La addition was increased to 4% wt The La-Sn phase diagram [37] reveals that Sn-rich La-Sn alloys consist of a La + $La_5Sn_3$ solid solution at room temperature and that eutectic melting occurs at 747 °C with a eutectic composition of 11.5% wt La and 88.5% wt Sn. Therefore, it is thought that the $La_5Sn_3$ phase is formed when the La content is over a certain amount and is solidified at roughly 740 °C, during the solidification of the Mg5Sn4La alloy. Thus, the presence of this phase in the alloys is expected [44]. It is worth pointing out that this phase is not detected on alloys with lower La content. Also, it should be noted that the amount of $Mg_2Sn$ decreases with increased La content. Such behavior is attributed to the formation of the $Mg_{17}La_2$ phase rather than $Mg_2Sn$. It is worth noting that, the lattice parameters of the observed phases are consistent to those reported on the previous studies (Table 4).

EDS analysis of the Mg5Sn4La alloy (Fig. 7 and Table 5) demonstrated the homogeneous distribution of Sn and La through the microstructure. It is obviously seen that the bright constituent on Fig. 7 (Point 1) is enriched with Sn and La. Thus, it is thought that these are $La_5Sn_3$ particles previously detected on the XRD analysis. Also, it has been determined that intergranular regions have much higher amounts of La and Sn (Fig. 7, Point 3). Therefore, it is apparent that intermetallic phases nucleated on the intergranular regions, though the presence of Sn and La in the matrix (Fig. 7, Point 2) proves the dissolution of the Sn and La containing intermetallic phases in the α-Mg matrix [44]. As expressed in Fig. 2, the grain size of the alloy is not homogenous due to the distribution of La throughout the matrix and due to the

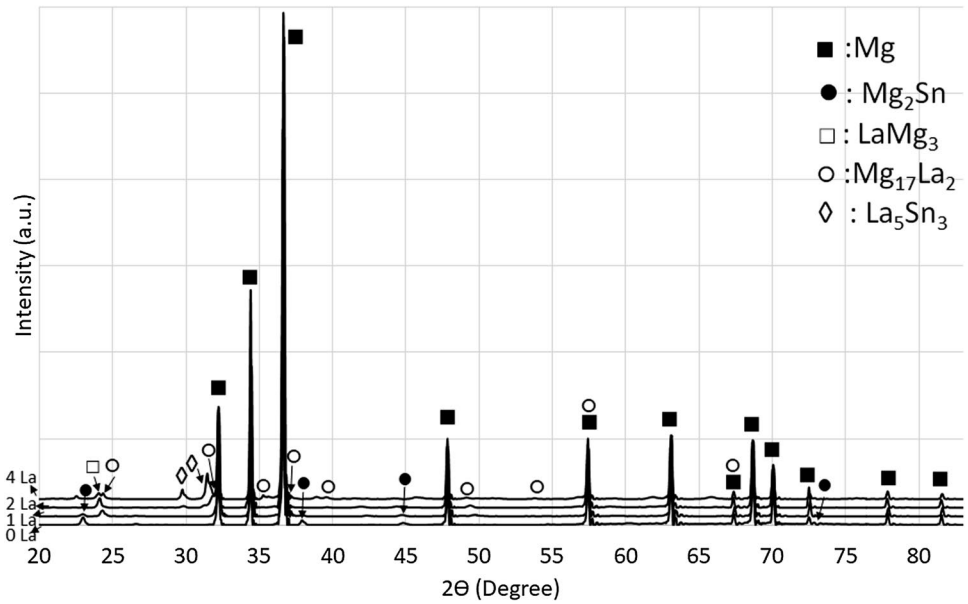


**Fig. 6** XRD patterns of the investigated alloys

**Table 4** Lattice parameters of the phases shown in Fig. 6

| Phase | Crystal Structure | Diffraction angle (degree) | Lattice Parameters (Å) | | Reference Lattice parameters (Å) | | |
|---|---|---|---|---|---|---|---|
| | | | a | c | a | c | References |
| $Mg_2Sn$ | Cubic | 22.98 | 6.738 | – | 6.765 | – | [50] |
| $Mg_{17}La_2$ | Hexagonal | 31.61 | 10.35 | 10.31 | 10.35 | 10.25 | [51] |
| $La_5Sn_3$ | Tetragonal | 31.45 | 12.70 | 6.43 | 12.74 | 6.34 | [52] |
| $LaMg_3$ | Cubic | 24.04 | 7.39 | – | 7.49 | – | [53] |

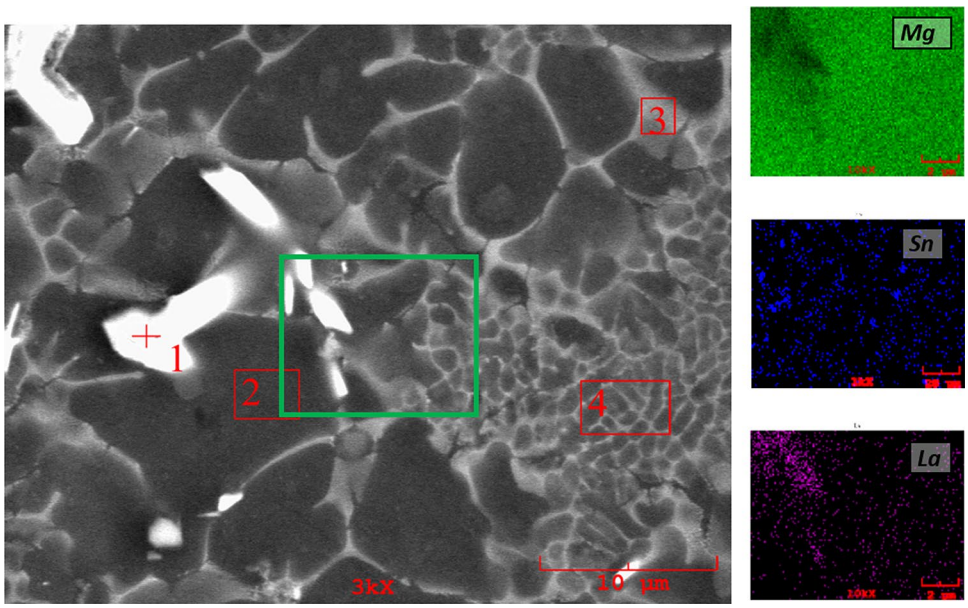


**Fig. 7** SEM image of the Mg2Sn4La alloy, and EDS elemental mapping analysis of the area represented with a green rectangle

different cooling rates because of the part geometry. Furthermore, the data collected showed that $Mg_{17}La_2$ and $La_5Sn_3$ are dominant phases in the Mg5Sn4La alloy.

The alloys tensile property data were determined as a function of La content and are displayed in Fig. 8. It is clearly seen from the stress–strain curves (Fig. 8-c) that both

**Table 5** EDX analysis results for locations shown in Fig. 7

| Point | Element (wt%) | | | |
|---|---|---|---|---|
| | Mg | Sn | La | O |
| 1 | 17.097 | 32.562 | 35.034 | 15.307 |
| 2 | 93.202 | 2.166 | 2.585 | 2.048 |
| 3 | 90.278 | 4.723 | 3.101 | 1.897 |
| 4 | 91.084 | 3.767 | 3.745 | 1.404 |

strength and ductility increases with increasing La content. Zhang and Muga [45] stated that alloying the Mg with Rare Earth elements causes such behavior. Guan et al. [46] observed that the $Mg_2Sn$ phase gradually refined, spherodized, and uniformly distributed with increasing La content. Mendis et al. [20] reported that La can facilitate the nucleation of Sn containing phases. Also, some specimens of the AZ91 alloy were produced using the same die-set and the same parameters for comparing the results. It is worth pointing out that although tensile strength of the AZ91 alloy is slightly higher than that of the Mg5Sn4La alloy its strain rate is as low as the 30% of the Mg5Sn4La alloy. It is reported that increasing Al content causes higher strength and good castability in the Al–Mg alloys preferred for industrial use. However, higher Al content is reported as being detrimental to ductility due to the higher amount of intermetallic phase of $Mg_{17}Al_{12}$ [19]. Thus, it is concluded that the presence of Al in the AZ91 alloys leads to lower strain rates because of the formation of the $Mg_{17}$ $Al_{12}$ intermetallic phase. The addition of 1% La did not cause a significant change; the tensile strength increased by 42% and 92%, respectively with the addition of 2% and 4% La. It is postulated that for the Mg5Sn2La alloy, the amount of the emerging phases (Fig. 6) is not enough to significantly change the properties. It should be noted that there is no tangible change in hardness with the addition of 2% and 4% La. However, the hardness of the Mg5Sn4La alloy is roughly 30% higher than that of the Mg5Sn alloy. Also, the ductility of the Mg5Sn alloy improved significantly with the addition of 4% La (Fig. 8-b). The increase in ductility upon the addition of 4% La to the base alloy is measured as 50%. Furthermore, the addition of La caused a linear increase in yield strength. It is thought that there are 2 possible mechanisms for strengthening of the base alloy with the addition of La. First is a decrease in grain size (Fig. 2). According to the Hall–Petch equation, lower grain sizes yield higher strength values [47]. Another reason for higher mechanical properties is the second-phase dispersoids observed in the alloys' microstructures [48]. As mentioned previously, the addition of La leads to the more fine and homogenous distribution of the $Mg_2Sn$ phase. A recent study showed that these $Mg_2Sn$ phases have a plate-shape morphology and form near α-Mg grain boundary and show growth perpendicular to the grain boundary [46]. Abbot et al. [19] reported that grain boundary sliding may be more dominant in the total deformation on the HPDC processed Mg alloys due to their smaller grain sizes. It is thought that plate-like $Mg_2Sn$ constituents hinder the sliding of the grain boundary by pinning the grain boundaries [33]. The mechanical properties of the base alloy are consistent with those of previous works [33, 41, 49].

## 4 Conclusions

This research aimed to investigate the effects of La addition on the properties of HPDC processed Mg-Sn alloys. Following are the accomplishments from the current work:

- Novel Mg–Sn–La alloys were successfully produced via the HPDC method and no macro defects were observed in the produced parts.
- The addition of La to the base alloy caused a decrease in the mean grain size due to the higher solidification temperature of La containing intermetallic phases. Furthermore, a more homogeneous grain size distribution was achieved by the addition of La to the Mg5Sn alloy.
- It is observed that Mg5Sn alloys comprise α-Mg and $Mg_2Sn$ phases. However, the addition of La to the base alloy provoked the formation of $LaMg_3$, $Mg_{17}La_2$ and $La_5Sn_3$ phases.
- Emerging phases caused higher tensile strength, ductility and hardness values due to their smaller grain size and dispersion strengthening. Mechanical characterization showed that the tensile strength of the base alloy was roughly doubled by adding 4% wt La. Also, yield strength and ductility of the Mg5Sn alloy increased by 25% and 50% respectively, in the mentioned circumstance.
- The room temperature tensile strength of the Mg5Sn4La alloy is similar to that of the AZ91 alloy; however, its strain rate is 300% higher. Higher ductility of the Mg–Sn–La alloys is attributed to the absence of the brittle $Mg_{17}Al_{12}$ phase.

In light of the results obtained, it can be concluded that the investigated alloys are good candidates for being alternative to the industrial Mg alloys and show good feasibility for production through the HPDC process.

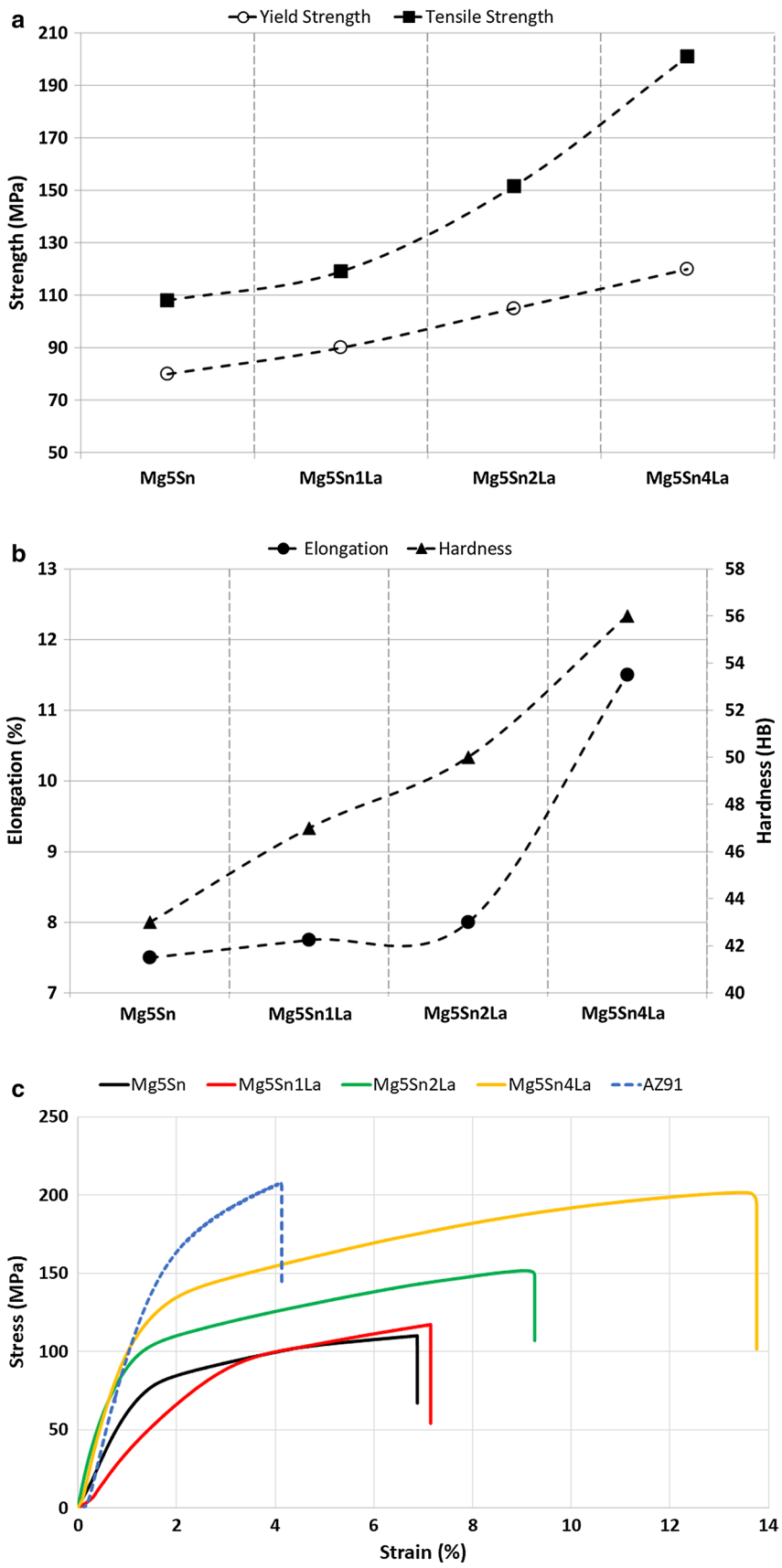


**Fig. 8** Mechanical properties of the investigated alloys, **a** yield strength and tensile strength, **b** elongation and hardness, **c** stress–strain curves

**Acknowledgements** This work was supported by the Sakarya University Scientific Research Project Council under Grant [number 2017-09-08-014]. The author also would like to acknowledge funding assistance provided by the Turkish National Scientific Council (Tubitak) via 2219 - International Postdoctoral Research Fellowship Program Grant no 1059B191800747. The help of İpek GÖKÇE, Murat GÖKÇE, Paramjot SINGH and Arulselvan ARUMUGHAM AKILAN in the experimental work are gratefully acknowledged.

## References

1. H.E. Friedrich, B.L. Mordike, editors, in (Springer, Berlin, 2006), pp. 499–632
2. F. Bonollo, N. Gramegna, G. Timelli, JOM **67**, 901 (2015)
3. H.I. Laukli, High Pressure Die Casting of Aluminium and Magnesium Alloys—Grain Structure and Segregation Characteristics, Norwegian University of Science and Technology, 2004
4. I. Polmear, D. StJohn, J.-F. Nie, M. Qian, *Light Alloy*, 5th edn. (Elsevier, Boston, 2017), pp. 1–29
5. B.L. Mordike, T. Ebert, Mater. Sci. Eng. A **302**, 37 (2001)
6. V.V. Ramalingam, P. Ramasamy, M. Das Kovukkal, G. Myilsamy, Met. Mater. Int. (2019)
7. L.-Y. Chen, J.-Q. Xu, H. Choi, M. Pozuelo, X. Ma, S. Bhowmick, J.-M. Yang, S. Mathaudhu, X.-C. Li, Nature **528**, 539 (2015)
8. EEA, EEA Report No 27/2016 Monitoring $CO_2$ Emissions from New Passenger Cars and Vans in 2016 (2016)
9. Ç. Özay, E.B. Gencer, A. Gökçe, J. Therm. Anal. Calorim. **134**, 23 (2018)
10. A. Gökçe, F. Findik, A.O. Kurt, Mater. Charact. **62**, 730 (2011)
11. H.W. Shin, Int. J. Precis. Eng. Manuf. **13**, 2011 (2012)
12. H. Liu, Y. Chen, Y. Tang, S. Wei, G. Niu, J. Alloys Compd. **440**, 122 (2007)
13. W.W. Jian, G.M. Cheng, W.Z. Xu, H. Yuan, M.H. Tsai, Q.D. Wang, C.C. Koch, Y.T. Zhu, S.N. Mathaudhu, Mater. Res. Lett. **1**, 61 (2013)
14. M.K. Kulekci, Int. J. Adv. Manuf. Technol. **39**, 851 (2008)
15. A. Luo, M.O. Pekguleryuz, J. Mater. Sci. **29**, 5259 (1999)
16. H. Baker, M.M. Avedesian (eds.), *ASM Specialty Handbook: Magnesium and Magnesium Alloys* (ASM International, Cleveland, 1999)
17. I.J. Polmear, Mater. Trans., JIM **37**, 12 (1996)
18. Y. Lü, Q. Wang, W. Ding, X. Zeng, Y. Zhu, Mater. Lett. **44**, 265 (2000)
19. T.B. Abbott, M.A. Easton, C.H. Caceres, in *Handbook of Mechanical Alloy Design*, ed. by G.E. Totten, L. Xie, K. Funatani (CRC Press, Boca Raton, 2004), pp. 487–538
20. C.L. Mendis, C.J. Bettles, M.A. Gibson, C.R. Hutchinson, Mater. Sci. Eng., A **435–436**, 163 (2006)
21. S. Tekumalla, S. Seetharaman, A. Almajid, M. Gupta, Metals (Basel). **5**, 1 (2014)
22. N. Hort, Y. Huang, D. Fechner, M. Störmer, C. Blawert, F. Witte, C. Vogt, H. Drücker, R. Willumeit, K.U. Kainer, F. Feyerabend, Acta Biomater. **6**, 1714 (2010)
23. S.M. Zhu, M.A. Gibson, M.A. Easton, J.F. Nie, Scr. Mater. **63**, 698 (2010)
24. N. Birbilis, M.A. Easton, A.D. Sudholz, S.M. Zhu, M.A. Gibson, Corros. Sci. **51**, 683 (2009)
25. S.M. Zhu, M.A. Gibson, J.F. Nie, M.A. Easton, G.L. Dunlop, Metall. Mater. Trans. A **40**, 2036 (2009)
26. T.L. Chia, M.A. Easton, S.M. Zhu, M.A. Gibson, N. Birbilis, J.F. Nie, Intermetallics **17**, 481 (2009)
27. S. Zhu, M.A. Easton, T.B. Abbott, J.F. Nie, M.S. Dargusch, N. Hort, M.A. Gibson, Metall. Mater. Trans. A Phys. Metall. Mater. Sci. **46**, 3543 (2015)
28. I.P. Moreno, T.K. Nandy, J.W. Jones, J.E. Allison, T.M. Pollock, Scr. Mater. **45**, 1423 (2001)
29. I.P. Moreno, T.K. Nandy, J.W. Jones, J.E. Allison, T.M. Pollock, Scr. Mater. **48**, 1029 (2003)
30. H. Da Zhao, G.W. Qin, Y.P. Ren, W.L. Pei, D. Chen, Y. Guo, Trans. Nonferrous Met. Soc. China **20**, s493 (2010)
31. Q. Wang, Y. Shen, B. Jiang, A. Tang, J. Song, Z. Jiang, T. Yang, G. Huang, F. Pan, Mater. Sci. Eng. A **735**, 131 (2018)
32. W. Ding, Y. Chen, S. Xiao, Z. Cui, P. Cheng, J. Rare Earths **35**, 585 (2017)
33. G. Yarkadaş, L.C. Kumruoğlu, H. Şevik, Mater. Charact. **136**, 152 (2018)
34. Z.H. Huang, W.H. Liu, W.J. Qi, J. Xu, J. Mater. Eng. **44**, 56 (2016)
35. J. Luo, R.S. Chen, E.H. Han, Mater. Sci. Forum **747–748**, 245 (2013)
36. J. Jiang, G. Bi, J. Liu, C.C. Ye, J. Lian, Z. Jiang, J. Magn. Alloys **2**, 257 (2014)
37. H. Okamoto, J. Phase Equilib. **23**, 289 (2002)
38. A. Bowles, K. Nogita, M. Dargusch, C. Davidson, J. Griffiths, Mater. Trans. **45**, 3114 (2004)
39. G.E. Lloyd, Miner. Mag. **51**, 3 (1987)
40. M. Mezbahul-Islam, A.O. Mostafa, M. Medraj, J. Mater. **2014**, 1 (2014)
41. M. Cong, Z. Li, J. Liu, X. Miao, B. Wang, Q. Xi, Russ. J. Non-Ferrous Met. **57**, 445 (2016)
42. A. Berche, P. Benigni, J. Rogez, M.-C. Record, J. Therm. Anal. Calorim. **107**, 797 (2012)
43. S. Wei, Y. Chen, Y. Tang, X. Zhang, M. Liu, S. Xiao, Y. Zhao, Mater. Sci. Eng. A **508**, 59 (2009)
44. Z. Zhao, P. Bai, R. Guan, V. Murugadoss, H. Liu, X. Wang, Z. Guo, Mater. Sci. Eng. A **734**, 200 (2018)
45. C.O. Muga, Z.W. Zhang, Adv. Mater. Sci. Eng. **2016**, 1 (2016)
46. R.G. Guan, Y.F. Shen, Z.Y. Zhao, R.D.K. Misra, Sci. Rep. **6**, 1 (2016)
47. G.E. Dieter, D.J. Bacon, *Mechanical Metallurgy* (McGraw-Hill, New York, 1986)
48. E. Hornbogen, J. Light Met. **1**, 127 (2001)
49. H. Liu, Y. Chen, Y. Tang, S. Wei, G. Niu, Mater. Sci. Eng. A **464**, 124 (2007)
50. V.K. Zaitsev, M.I. Fedorov, E.A. Gurieva, I.S. Eremin, P.P. Konstantinov, A.Y. Samunin, M.V. Vedernikov, Phys. Rev. B **74**, 2 (2006)
51. C.L. Mendis, C.J. Bettles, M.A. Gibson, S. Gorsse, C.R. Hutchinson, Philos. Mag. Lett. **86**, 443 (2006)
52. E. Franceschi, J. Less-Common Met. **66**, 175 (1979)
53. M. Wang, R. Pan, P. Li, N. Bian, B. Tang, L. Peng, W. Ding, J. Cent, S. Univ. **21**, 2136 (2014)